J. Fluid Mech. (2009), *vol.* 633, *pp.* 449–460.
doi:10.1017/S0022112009990528 Printed in the United Kingdom

Mean temperature profiles in turbulent Rayleigh–Bénard convection of water

OLGA SHISHKINA[1]† AND ANDRÉ THESS[2]

[1]DLR – Institute for Aerodynamics and Flow Technology, Bunsenstrasse 10, 37073 Göttingen, Germany

[2]Institute of Thermodynamics and Fluid Mechanics, Ilmenau University of Technology, P.O. Box 100565, 98684 Ilmenau, Germany

(Received 28 January 2009 and in revised form 17 May 2009)

We report an investigation of temperature profiles in turbulent Rayleigh–Bénard convection of water based on direct numerical simulations (DNS) for a cylindrical cell with unit aspect ratio for the same Prandtl number Pr and similar Rayleigh numbers Ra as used in recent high-precision measurements by Funfschilling *et al.* (*J. Fluid Mech.*, vol. 536, 2005, p. 145). The Nusselt numbers Nu computed for $Pr = 4.38$ and $Ra = 10^8$, 3×10^8, 5×10^8, 8×10^8 and 10^9 are found to be in excellent agreement with the experimental data corrected for finite thermal conductivity of the walls. Based on this successful validation of the numerical approach, the DNS data are used to extract vertical profiles of the mean temperature. We find that near the heating and cooling plates the non-dimensional temperature profiles $\Theta(y)$ (where y is the non-dimensional vertical coordinate), obey neither a logarithmic nor a power law. Moreover, we demonstrate that the Prandtl–Blasius boundary layer theory cannot predict the shape of the temperature profile with an error less than 7.9 % within the thermal boundary layers (TBLs). We further show that the profiles can be approximated by a universal stretched exponential of the form $\Theta(y) \approx 1 - \exp(-y - 0.5y^2)$ with an absolute error less than 1.1 % within the TBLs and 5.5 % in the whole Rayleigh cell. Finally, we provide more accurate analytical approximations of the profiles involving higher order polynomials in the approximation.

1. Introduction

In the past decades Rayleigh–Bénard convection (RBC) has been investigated intensively in many theoretical and experimental studies (for reviews we refer to Siggia 1994; Bodenschatz, Pesch & Ahlers 2000; Kadanoff 2001; Ahlers, Grossmann & Lohse 2009), as well as in numerous numerical works such as Kerr (1996), Verzicco & Camussi (2003), Amati *et al.* (2005), Calzavarini *et al.* (2005), Hartlep, Tilgner & Busse (2005), Kenjereš & Hanjalić (2006), Sergent, Joubert & Le Quéré (2006), Shishkina & Wagner (2007), Shishkina & Wagner (2008), van Reeuwikj, Jonker & Hanjalić (2008*a*, *b*), Emran & Schumacher (2008) and Kaczorowski & Wagner (2009). In spite of significant progress achieved in understanding of the nature of RBC, several important questions are still open. One of them is whether the vertical profiles of the mean temperature in turbulent RBC can be described by simple and universal analytical expressions.

† Email address for correspondence: Olga.Shishkina@dlr.de

Several works (Tilgner, Belmonte & Libchaber 1993; Lui & Xia 1998; Hölling & Herwig 2006; du Puits *et al* 2007) were devoted to the investigation of the temperature profiles in turbulent RBC. In certain subregions of the thermal boundary layers (TBLs), the profiles were shown to follow a power law scaling (du Puits *et al* 2007) or a logarithmic dependence (Hölling & Herwig 2006). However, no universal approximations which represent the temperature distributions in the vertical direction in the whole region of interest, namely, from the heating or cooling plate up to the central plane, or at least within the TBL alone, were found so far. In the present work we address the question to what extent the temperature profiles in turbulent convection of water have a simple and universal shape. The work is based on our direct numerical simulations (DNS) of turbulent RBC for $Pr = 4.38$ and Ra up to 10^9, which are similar to those considered in recent accurate measurements in water by Funfschilling *et al.* (2005).

The paper is organized as follows. Section 2 is devoted to the governing equations and some details on the DNS. In § 3 we compare our numerically computed Nu with those obtained in the measurements, in order to validate the DNS data. The temperature profiles in the vertical direction are analysed and approximated in § 4. Section 5 summarizes our conclusions.

2. Governing equations and numerical method

We consider RBC of water in a cylindrical cell with equal height H and diameter D, i.e. with aspect ratio $\Gamma = D/H = 1$. The system of the governing momentum, energy and continuity equations for the non-dimensional velocity $\boldsymbol{u}$, temperature T and pressure p in the framework of the Boussinesq approximation reads

$$\begin{aligned} \partial \boldsymbol{u}/\partial t + \boldsymbol{u}\cdot\nabla\boldsymbol{u} + \nabla p &= Ra^{-1/2}Pr^{1/2}\Delta\boldsymbol{u} + T\boldsymbol{e}_z, \\ \partial T/\partial t + \boldsymbol{u}\cdot\nabla T &= Ra^{-1/2}Pr^{-1/2}\Delta T, \\ \nabla\cdot\boldsymbol{u} &= 0. \end{aligned} \tag{2.1}$$

The equations are supplemented by the boundary conditions $T = 0.5$ at the heating plate ($z = 0$, $0 \leqslant r \leqslant 0.5$), $T = -0.5$ at the cooling plate ($z = 1$, $0 \leqslant r \leqslant 0.5$), $\partial T/\partial r = 0$ at the lateral wall ($r = 0.5$, $0 \leqslant z \leqslant 1$) as well as the no-slip condition $\boldsymbol{u} = 0$ at all boundaries. The equations have been made non-dimensional by using H, $(\alpha g H(T_H - T_C))^{1/2}$, $H(\alpha g H(T_H - T_C))^{-1/2}$, and $T_H - T_C$ as units of length, velocity, time and temperature, respectively. The Rayleigh and Prandtl numbers are defined as $Ra = \alpha g H^3(T_H - T_C)/(\nu\kappa)$ and $Pr = \nu/\kappa$, respectively, where α is the isobaric thermal expansion coefficient, g the acceleration of gravity, ν the kinematic viscosity, κ the thermal diffusivity, T_H the temperature of the heating plate and T_C the temperature of the cooling plate. Cylindrical coordinates (r, ϕ, z) are used.

We perform DNS of turbulent RBC for $Pr = 4.38$ which is identical to that in the experiments of Funfschilling *et al.* (2005). We consider five Rayleigh numbers, namely $Ra = 10^8$, 3×10^8, 5×10^8, 8×10^8 and 10^9, which are in the same range as the mentioned experiments. For each simulation we compute the time-averaged Nusselt number Nu, the horizontally averaged profiles of the temperature $\overline{T}(z)$ and of the r.m.s. temperature fluctuations $\overline{T}_{rms}(z)$. Here the overbar denotes time- and area-averaging over a horizontal plane at a distance z from the bottom plate. The simulations were performed using a computational code based on a fourth order accurate finite volume method for solving the system (2.1) in cylindrical coordinates

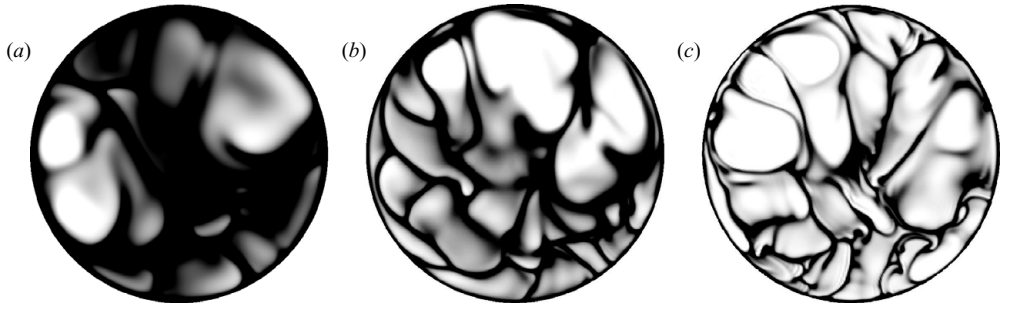

FIGURE 1. Snapshots of the temperature fields in a horizontal cross-section at distance $z = 10^{-2}$ from the bottom plate as obtained in the DNS of turbulent RBC in a cylindrical container with the aspect ratio $\Gamma = 1$ for $Pr = 4.38$ and (*a*) $Ra = 10^8$, (*b*) $Ra = 3 \times 10^8$ and (*c*) $Ra = 10^9$. The corresponding TBL thicknesses are (*a*) 1.5×10^{-2}, (*b*) 1.1×10^{-2} and (*c*) 7.8×10^{-3}. The same grey scale ranges from white (low temperatures) to black (high temperatures).

on staggered structured non-equidistant grids. The current version of the code is described in Shishkina, Shishkin & Wagner (2009).

The computational mesh consists of $220 \times 512 \times 96$ nodes in the vertical, azimuthal and radial directions, respectively, which are distributed equidistantly in the azimuthal direction and are clustered in the vicinity of the rigid walls to resolve viscous and TBLs. An *a posteriori* analysis of the mesh resolution was conducted as in Shishkina & Wagner (2008) and confirmed that in all discussed DNS the mesh satisfies the spatial resolution requirements by Grötzbach (1983), both in the bulk and in the vicinity of the rigid walls. Hence, it is fine enough to resolve all relevant turbulent scales. Namely, in all DNS the mesh satisfies the requirement $h_{V_i} \leqslant \pi \eta_{V_i}(Ra) Pr^{-3/4}$ on each finite volume V_i, where h_{V_i} is the mesh width, $\eta_{V_i}(Ra) = Ra^{-3/8} Pr^{3/8} \epsilon_u^{-1/4}$ is the smallest Kolmogorov scale on V_i and ϵ_u is the rate of turbulent kinetic energy dissipation.

Figure 1 illustrates the DNS data with the instantaneous temperature distributions in a horizontal cross-section at a distance $z = 10^{-2}$ from the bottom for the cases $Ra = 10^8$, 3×10^8 and 10^9. These snapshots reflect sheet-like flow structures close to the plates, which are similar to those obtained experimentally by Zhou, Sun & Xia (2007).

3. Mean heat flux

First, we focus our attention to the Nusselt number which is a dimensionless measure of the mean heat flux. We have deliberately chosen Pr and Ra such that we can directly compare our Nusselt numbers to those obtained in a series of recent high-accuracy experiments in water performed by Funfschilling *et al.* (2005). In our normalization $Nu = Ra^{1/2} Pr^{1/2} \overline{u_z T} - \partial \overline{T} / \partial z$. The DNS data were collected during τ dimensionless time units, which together with the maximum relative variation e of the Nusselt numbers computed at different heights $z \in [0, 1]$ are given below. The following mean Nu were obtained: $Nu = 32.5$ ($Ra = 10^8$, $\tau = 64$, $e = 1.7\,\%$), $Nu = 44.8$ ($Ra = 3 \times 10^8$, $\tau = 151$, $e = 1.3\,\%$), $Nu = 52.3$ ($Ra = 5 \times 10^8$, $\tau = 205$, $e = 0.6\,\%$), $Nu = 60.0$ ($Ra = 8 \times 10^8$, $\tau = 267$, $e = 0.9\,\%$) and $Nu = 64.2$ ($Ra = 10^9$, $\tau = 290$, $e = 0.9\,\%$).

In figure 2 the Nusselt numbers are presented as they were obtained in the DNS together with the experimental results for the same $Pr = 4.38$ and the same

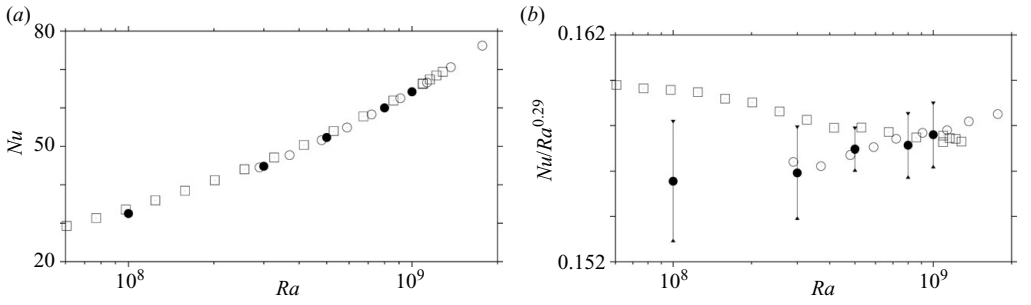

FIGURE 2. (*a*) Validation of the DNS: Nusselt numbers for turbulent RBC in water ($Pr = 4.38$) in cylindrical cells with the aspect ratio $\Gamma = 1$ as obtained in the DNS (●), compared to the experimental data of Funfschilling *et al.* (2005) for their small ($D = 9.21$ cm, □) and medium ($D = 24.84$ cm, ○) cells. The experimental data have been corrected for the sidewall conductance, according to Ahlers (2000). (*b*) Compensated Nusselt numbers $Nu/Ra^{0.29}$ for the same data as in (*a*). The vertical bars show the variation of the Nusselt numbers computed at different distances from the bottom.

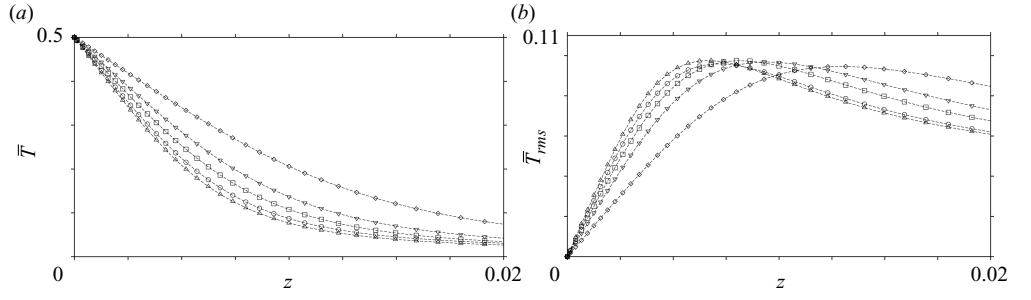

FIGURE 3. (*a*) Temperature profiles and (*b*) r.m.s. temperature fluctuations in the vertical direction near the bottom plate, averaged over horizontal plane, as obtained in the DNS of turbulent RBC for $Pr = 4.38$, $\Gamma = 1$ and $Ra = 10^8(\diamond)$, $3 \times 10^8(\triangledown)$, $5 \times 10^8(\square)$, $8 \times 10^8(\circ)$ and $10^9(\triangle)$.

cylindrical geometry of the container with $\Gamma \approx 1$. The measurements were conducted by Funfschilling *et al.* (2005) in their small ($D = 9.21$ cm) and medium ($D = 24.84$ cm) apparatus using water with the mean temperature T_m about 40 °C.

One can see that the obtained numerical data are generally in excellent agreement with the measurements in the medium apparatus, in which the Oberbeck–Boussinesq assumptions were fulfilled for all considered Ra. The results shown in figure 2 can be accepted as a successful validation of the numerical code. We can now use the numerical data to extract information that is not available in the experiments.

4. Temperature profiles

It is known from previous works that the mean temperature profiles in RBC change dramatically in thin TBLs with a non-dimensional thickness $\lambda = 0.5/Nu$, while in core regions they are nearly independent from the vertical coordinate z. In figure 3 we show the mean temperature and r.m.s. temperature fluctuations averaged over a horizontal plane as functions of z. The steepening of the profiles near the bottom, depending on Ra, is well seen in figure 3(*a*). With increasing Ra, the TBL thickness decreases and the point of maximum of the r.m.s. temperature fluctuations moves towards the plate.

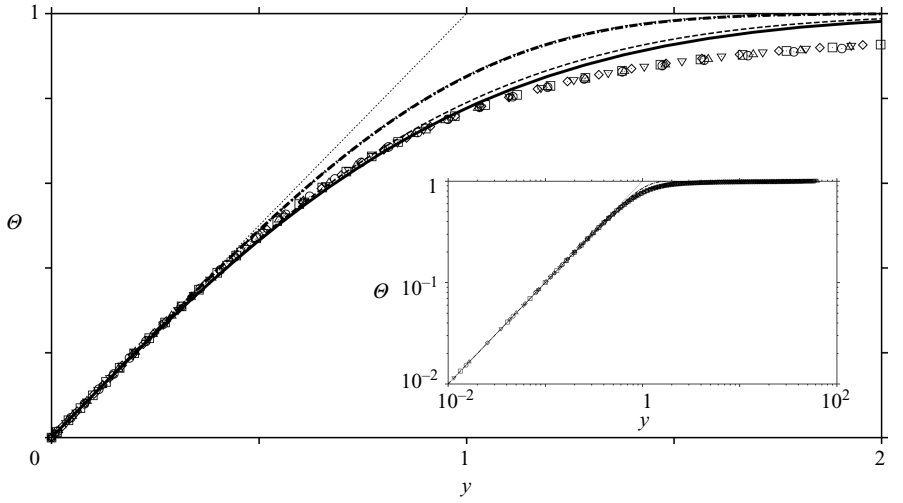

FIGURE 4. Scaled temperature profiles $\Theta(y)$ defined by (4.1), as obtained in the DNS of turbulent RBC for $Pr = 4.38$, $\Gamma = 1$ and $Ra = 10^8(\diamond)$, $3 \times 10^8(\triangledown)$, $5 \times 10^8(\square)$, $8 \times 10^8(\circ)$ and $10^9(\triangle)$. The slope of $\Theta(y)$ at $y = 0$ $(\cdots)$ is shown as well as Prandtl–Blasius approximation (4.5), (4.7) $(- \cdot -)$ and approximations (4.11) (——) and (4.9) for $\omega = 2$ $(- - -)$ and $\omega = 3$ (- - -). For $\omega = 3$ (- - -) approximation (4.9) coincides with Prandtl–Blasius approximation (4.5) $(- \cdot -)$ and for $\omega = 2$ $(- - -)$ it is close to approximation (4.11) (——). Inset shows Θ profiles in double-logarithmic scale. Approximation (4.11) (——) represents very precisely (with the maximum absolute error less than 1.1 %) the profiles within the whole interval $y \in [0, 1]$ which corresponds to the TBL.

In order to compare profiles for different Ra, we consider the function

$$\Theta(y) = 1 - 2\overline{T}, \qquad \text{with } y = 2\,Nu\,z. \tag{4.1}$$

The introduction of the inner variable y takes into account that the TBL thickness is determined by Nu. As it is seen in figure 4, the functions $\Theta(y)$ are very similar to each other in spite of the differences in Ra, at least in the considered interval $10^8 \leqslant Ra \leqslant 10^9$. Also y-dependent non-dimensional conductive heat fluxes $\mathrm{d}\Theta/\mathrm{d}y$, which are presented in figure 5(a), look very similar for different Ra. In particular, $\mathrm{d}\Theta/\mathrm{d}y$ equals 90 % of its initial value for $\Theta = 0.37$ and falls to 50 % of its initial value for $\Theta = 0.67$.

Such a collapse of the data for different Ra, presented in figures 4 and 5(a), was expected, since independently from Ra the function $\Theta(y)$ must satisfy the following requirements. At $y = 0$ the next three equalities are true:

$$\Theta = 0, \quad \mathrm{d}\Theta/\mathrm{d}y = 1, \quad \mathrm{d}^2\Theta/\mathrm{d}y^2 = 0 \quad \text{for } y = 0. \tag{4.2}$$

(The first two follow from (4.1) and the definition of the Nusselt number, while the last one is the energy equation at the horizontal plate.) For high values of y, i.e. in the bulk of the cell, the function $\Theta(y)$ must satisfy

$$\Theta \to 1, \quad \mathrm{d}\Theta/\mathrm{d}y \to 0, \quad \mathrm{d}^2\Theta/\mathrm{d}y^2 \to 0 \quad \text{for } y \to \infty. \tag{4.3}$$

Our objective is to find accurate approximations of $\Theta(y)$ within the TBLs ($0 \leqslant y \leqslant 1$) and in the whole Rayleigh cell ($0 \leqslant y \leqslant Nu$).

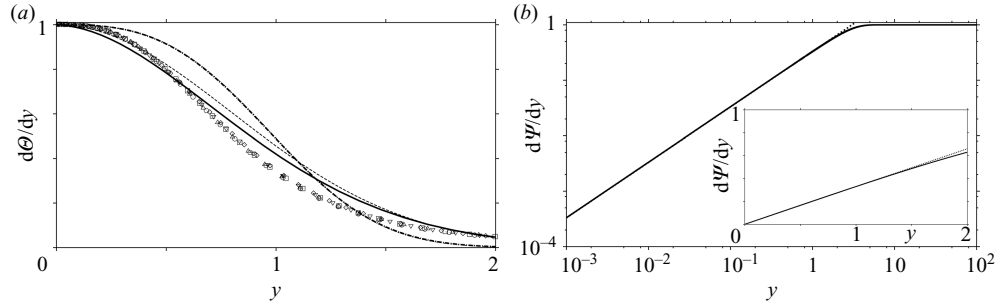

FIGURE 5. (*a*) $\mathrm{d}\Theta/\mathrm{d}y$ defined by (4.1) as obtained in the DNS of turbulent RBC for $Pr = 4.38$, $\Gamma = 1$ and $Ra = 10^8(\diamond)$, $3 \times 10^8(\triangledown)$, $5 \times 10^8(\square)$, $8 \times 10^8(\circ)$ and $10^9(\triangle)$ and from Prandtl–Blasius approximation (4.5), (4.7) (—·—) and approximations (4.11) (——) and (4.9) for $\omega = 2$ (– – –) and $\omega = 3$ (- - -). For $\omega = 3$ (- - -) approximation (4.9) coincides with Prandtl–Blasius approximation (4.5) (— · —). (*b*) Longitudinal velocity profile $\mathrm{d}\Psi/\mathrm{d}y$ in double-logarithmic and ordinary scales (inset) as obtained using the Prandtl–Blasius equations (4.4) and (4.6). Within the TBL ($y \in [0, 1]$) the function $\mathrm{d}\Psi/\mathrm{d}y$ is almost linear in y (compare with a dashed straight line).

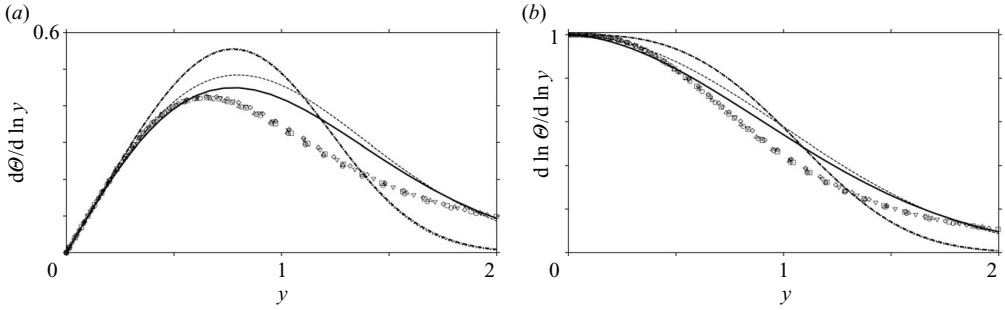

FIGURE 6. Diagnostic functions (*a*) $\mathrm{d}\Theta/\mathrm{d}\ln y$ (for logarithmic profiles) and (*b*) $\mathrm{d}\ln\Theta/\mathrm{d}\ln y$ (for power-law profiles) as obtained from the DNS of RBC for $Pr = 4.38$, $\Gamma = 1$ and $Ra = 10^8(\diamond)$, $3 \times 10^8(\triangledown)$, $5 \times 10^8(\square)$, $8 \times 10^8(\circ)$ and $10^9(\triangle)$ and using Prandtl–Blasius approximation (4.5), (4.7) (— · —) and approximations (4.11) (——) and (4.9) for $\omega = 2$ (– – –) and $\omega = 3$ (- - -). For $\omega = 3$ approximation (4.9) coincides with Prandtl–Blasius approximation (— · —).

4.1. *Power-law profile versus logarithmic profile*

The question, whether velocity profiles in shear flows obey a power-law or a logarithmic shape, has been intensively debated in the past (see Buschmann & Gad-el-Hak 2003). Our DNS enable us to address the analogous issue for the temperature profiles in RBC.

To analyse, whether $\Theta(y)$ obeys a logarithmic or a power-law (as it was obtained in some experimental studies, e.g. by du Puits *et al* 2007), we evaluate the diagnostic functions $\mathrm{d}\ln\Theta/\mathrm{d}\ln y$ and $\mathrm{d}\Theta/\mathrm{d}\ln y$ (see e.g. Zanoun, Durst & Nagib 2003). If the profile can be approximated by a power law of the form $\Theta \sim y^\gamma$, the power-law diagnostic function $\mathrm{d}\ln\Theta/\mathrm{d}\ln y$ must have a plateau in a certain interval of y. If the profile obeys a logarithmic shape, i.e. $\Theta \sim \ln(y)$, $\mathrm{d}\Theta/\mathrm{d}\ln y$ must have a certain plateau.

In figure 6(*a*) the diagnostic function for logarithmic behaviour is presented as it was evaluated from the DNS data. This function is non-monotonic and exhibits a maximum near $y = 0.65$. The interval of relatively large values of $\mathrm{d}\Theta/\mathrm{d}\ln y$ is

not sufficiently broad to consider it as a plateau. We can therefore conclude that for the considered Ra there is no logarithmic scaling of the profiles as it could be expected from the boundary layer (BL) theories under assumptions that the TBLs are turbulent. This fact is not surprising, since the Reynolds numbers within the TBLs are small, although the flow in the bulk is turbulent.

Figure 6(b) shows that in contrast to the logarithmic diagnostic function, the power-law diagnostic function decreases monotonically from the value 1 near the wall to zero without any tendency for the formation of a plateau. Therefore, for the considered parameter range, $\Theta(y)$ cannot be considered as a power-law profile either.

From the above discussion it follows that one has to seek approximations of the function $\Theta(y)$, which are more sophisticated than simple power laws or logarithmic dependencies.

4.2. *Approximation derived from the boundary layer theories*

The Reynolds numbers within the TBLs in RBC are known to be small (see e.g. Ahlers *et al.* 2009), therefore we first compare the temperature profiles obtained in the DNS with those derived from the Prandtl–Blasius BL equations (see the theory by Grossmann & Lohse 2000 and Schlichting & Gersten 2000). According to the theory, the similarity streamfunction $\Psi(\xi)$ and temperature profile $\Theta(\xi)$ can be obtained from the following system of ordinary differential equations:

$$\mathrm{d}^3\Psi/\mathrm{d}\xi^3 + 0.5\,\Psi\,\mathrm{d}^2\Psi/\mathrm{d}\xi^2 = 0, \tag{4.4}$$

$$\mathrm{d}^2\Theta/\mathrm{d}\xi^2 + 0.5\,Pr\,\Psi\,\mathrm{d}\Theta/\mathrm{d}\xi = 0, \tag{4.5}$$

with respect to the similarity variable $\xi = z/l$, where l is a certain length scale. For (4.4) and (4.5), one has, respectively, the following boundary conditions:

$$\Psi(0) = 0, \quad \mathrm{d}\Psi/\mathrm{d}\xi(0) = 0, \quad \mathrm{d}\Psi/\mathrm{d}\xi(\infty) = 1, \tag{4.6}$$

$$\Theta(0) = 0, \quad \Theta(\infty) = 1. \tag{4.7}$$

We solve numerically (4.4), (4.6) and further (4.5), (4.7), using the shooting method. In particular, for the function Θ for $Pr = 4.38$ at $\xi = 0$ we get $\mathrm{d}\Theta/\mathrm{d}\xi = C^{-1}$ with $C \approx 1.8139$. Since both, the similarity variable ξ and the inner variable y, are linearly dependent on the distance from the horizontal plate, from the last relation and $\mathrm{d}\Theta/\mathrm{d}y = 1$ at $y = 0$ we obtain that the variables ξ and y are related to each other as follows:

$$\xi = Cy, \tag{4.8}$$

(and $\xi = C$ corresponds to the border between the TBL and the bulk). The functions $\Theta(y)$ and $\mathrm{d}\Psi/\mathrm{d}y(y)$ are plotted in figures 4 and 5(b), respectively. One can see that for $Pr = 4.38$ the function $\mathrm{d}\Psi/\mathrm{d}y$, which is proportional to the horizontal velocity, is almost linear within the TBL ($y \in [0, 1]$).

On the other hand, in the boundary layer theories developed by Landau & Lifshitz (1959) and by Shraiman & Siggia (1990) (based on the measurements of Castaing *et al.* 1989), the horizontal velocity is also assumed to be linear in y close to the plate. From this, following Shraiman & Siggia (1990), one derives $\mathrm{d}\Theta/\mathrm{d}y = \exp(-By^3)$ with a certain coefficient B.

In order to find a better fit to the mean temperature profiles, we can further introduce a parameter $\omega \in [2, 3]$ in the approximation

$$\mathrm{d}\Theta/\mathrm{d}y = \exp(-By^{\omega}), \quad \text{i.e. } \Theta(y) = \int_0^y \exp(-B\zeta^{\omega})\,\mathrm{d}\zeta, \tag{4.9}$$

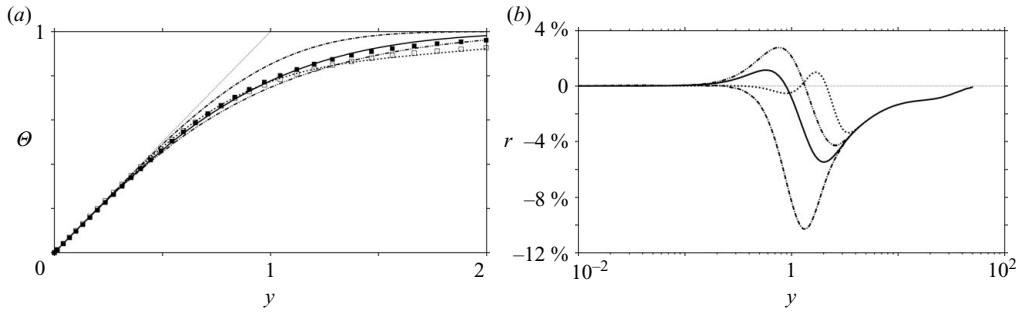

FIGURE 7. (*a*) $\Theta(y)$ defined by (4.1), as obtained in the DNS of RBC for $Pr = 4.38$, $\Gamma = 1$ and 5×10^8 (symbols) together with the slope of $\Theta(y)$ at $y = 0$ (straight line), Prandtl–Blasius approximation (4.5), (4.7) ($-\cdot-$) and approximations (4.11) (——) and (4.10) for $N = 1$ ($-\cdot\cdot-$) and $N = 2$ ($\cdots$). The surface-averaged temperature profile (□) deviates from the Prandtl–Blasius approximation ($-\cdot-$) more significantly than the profile at the centreline of the cell (■). (*b*) Approximation errors for Prandtl–Blasius approximation (4.5) ($-\cdot-$) and approximations (4.11) (——) and (4.10) for $N = 1$ ($-\cdot\cdot-$) and $N = 2$ ($\cdots$). Region $y \in [0, 1]$ corresponds to the TBL.

(which can be derived from a certain assumption that the horizontal velocity is proportional to $y^{\omega-2}$ in some part of the TBL). For any ω the constant B in (4.9) can be computed from the requirement $\Theta(\infty) = 1$. In the case $\omega = 3$, considered by Shraiman & Siggia (1990) and Chilla *et al* (1993), we obtain $B \approx 0.71207$. In the limit case $\omega \to 2$ we obtain $B = \pi/4$, since for $y \to \infty$ the temperature profile $\Theta(y)$ is reduced to the Gaussian integral, namely $\Theta(\infty) = \int_0^\infty \exp(-(\pi/4)\zeta^2)\,\mathrm{d}\zeta = 1$.

In figures 4–6 Prandtl–Blasius approximation (4.5), (4.7) and approximations (4.9) for $\omega = 2$ and $\omega = 3$ of $\Theta(y)$ are presented together with the functions derived from $\Theta(y)$. These approximations reflect in principle the behaviour of the temperature profiles and the diagnostic functions (see also the distribution of the approximations errors in figure 7(*b*) and table 2). Prandtl–Blasius approximation (4.5), (4.7) almost replicates approximation (4.9) for $\omega = 3$, since in the considered case of water in both approximations the horizontal velocity is either shown to be or assumed to be linear in y within the TBL.

The constant C in (4.8) depends generally on Pr and decreases to 1 with growing Pr. Hence, with increasing Pr the border of the TBL ($y = 1$ or $\xi = C$) moves towards the plate, i.e. to the left in figure 5(*b*), where $\mathrm{d}\Psi/\mathrm{d}y$ displays a perfectly linear behaviour. From this one concludes that for high Pr (larger than $Pr = 4.38$) Prandtl–Blasius approximation (4.5), (4.7) should become even closer to approximation (4.9) with $\omega = 3$.

The temperature profiles computed at the centreline of the cell generally differ from the surface-averaged profiles (see figure 7*a*). For all considered Ra the surface-averaged profiles deviate from Prandtl–Blasius approximation (4.5), (4.7) and approximations (4.9) more significantly than the centreline profiles. This might be explained by the fact that none of the considered BL theories takes into account the thermal plumes activity, which in the case of $\Gamma = 1$ and high Ra is known to be weaker in the centre of the cell and stronger close to the vertical walls.

4.3. *Further analytical approximation of the temperature profiles*

Theoretically, one can use any full functional basis to approximate $\Theta(y)$. However, a large number of expansion terms are usually required to obtain an approximation which accurately represents the temperature profiles close to the plate as well as in the

		Ra				
N	a_i	10^8	3×10^8	5×10^8	8×10^8	10^9
1	a_1	0.1313	0.1262	0.1317	0.1460	0.1436
2	a_1	−0.3643	−0.3645	−0.3751	−0.3950	−0.3766
2	a_2	0.3842	0.3786	0.3896	0.4146	0.3974

TABLE 1. Best-fit coefficients in the approximation (4.10), as calculated from a least-square fit to the numerically obtained temperature profiles Θ within the interval $0 \leqslant y \leqslant Nu$.

bulk. Further, analysing the diagnostic functions (as in figure 6), one can conjecture that $\Theta(y)$ has an exponential behaviour close to the plate. Finally, the Gaussian-like functions (4.9) are known to be well approximated by exponential functions.

In view of the above we seek a formal approximation of $\Theta(y)$ within the interval $y \in [0, Nu]$ in the following form

$$\Theta \approx 1 - \left(1 + \sum_{i=1}^{N} a_i y^{i+2}\right) \exp(-y - 0.5y^2), \tag{4.10}$$

which satisfies automatically the requirements (4.2) and (4.3) and the best-fit expansion coefficients a_i of which can be determined using additional information about the spatial temperature distribution, obtained numerically or experimentally.

It is worth to note that introduction of higher order polynomials under the exponential can give more accurate approximations within the TBL $y \in [0, 1]$, but does not lead to significantly better approximations within the whole interval $y \in [0, Nu]$, since the requirements (4.3) are not always fulfilled. Further, one can consider an approximation $\Theta \approx 1 - (1 - 0.5y^2 + \sum_{i=1}^{N} b_i y^{i+2}) \exp(-y)$, which also satisfies automatically the requirements (4.2) and (4.3), but for a fixed N and the best-fit coefficients a_i and b_i, $i = 1, \ldots, N$, the last approximation is generally less accurate than approximation (4.10).

If no additional information about the mean temperature distribution (except the Nusselt number) is provided, one can put to zero all the coefficients $a_i = 0, i = 1, \ldots, N$, in approximation (4.10) and thus obtain the following simplest universal exponential approximation of the mean temperature profiles

$$\Theta \approx 1 - \exp(-y - 0.5y^2). \tag{4.11}$$

It is remarkable that this universal (without any degrees of freedom) approximation (4.11) predicts very accurately the mean temperature profiles within the TBLs ($0 \leqslant y \leqslant 1$) with the maxima of the absolute error less than 1.1 %. More surprising is that this approximation represents well the profiles within the whole Rayleigh cell ($0 \leqslant y \leqslant Nu$) with the absolute error not more than 5.5 % for all considered Ra. The maximum of the absolute error of the approximation (4.11) is observed at $y \approx 2$.

To obtain best-fit coefficients for higher order approximations (4.10) of $\Theta(y)$ for $y \in [0, Nu]$, we use the least squares method to fit the DNS data. The obtained coefficients and the corresponding maxima of the absolute approximation errors are only weakly dependent on Ra. The obtained coefficients for these approximations are listed in table 1.

For the case $Ra = 5\times10^8$ table 2 presents the maxima of the absolute errors for Prandtl–Blasius approximation (4.5), (4.7) and approximations (4.11) and (4.10) with $N = 1$ and $N = 2$ degrees of freedom, over the whole region $0 \leqslant y \leqslant Nu$ and

	Error of approximation			
Interval	(4.5), (4.7)	(4.11)	(4.10), $N=1$	(4.10), $N=2$
Thermal boundary layers, $y \in [0, 1]$	7.9 %	1.1 %	2.8 %	0.5 %
Whole Rayleigh cell, $y \in [0, Nu]$	10.3 %	5.5 %	4.3 %	3.4 %

TABLE 2. Maximum absolute errors of the Prandtl–Blasius approximation (4.5), (4.7) and approximations (4.10), (4.11) of the scaled temperature profile Θ for $Ra = 5 \times 10^8$.

in particular subdomain $0 \leqslant y \leqslant 1$, which corresponds to the TBL. Error spatial distributions are also illustrated by figure 7(*b*).

5. Conclusions

Based on our accurate DNS data for turbulent RBC of water, $Pr = 4.38$, in a cylindrical cell with unit aspect ratio for different Ra up to 10^9, we evaluate time- and area-averaged temperature profiles $\Theta(y)$ (4.1), which depend on the vertical coordinate normalized with Nu. Within the TBLs the evaluated profiles are shown to support neither logarithmic nor power but exponential law.

It is shown that Prandtl–Blasius approximation (4.5), (4.7) of the mean temperature profiles in water produces absolute errors about 8 % within the TBLs alone and more than 10 % in the whole Rayleigh cell. For all considered Ra the surface-averaged temperature profiles deviate from the Prandtl–Blasius approximation more significantly than the profiles computed at the centreline of the cell. It is proved that for Prandtl numbers of order 1 and higher Prandtl–Blasius approximation (4.5), (4.7) almost coincides with approximation (4.9) for $\omega = 3$, i.e. $\Theta(y) \approx \int_0^y \exp(-0.71207\zeta^3)\,\mathrm{d}\zeta$.

For all considered Ra the simplest exponential approximation (4.11) without any degrees of freedom predicts the mean temperature profiles already with high accuracy, namely, with the maximum absolute errors less than 1.1 % and 5.5 % within the TBLs and in the whole convection cell, respectively. This means that knowing only Nu, one can predict the mean temperature distribution in the vertical direction with such accuracy.

To approximate the mean temperature profiles even more accurately in the whole region from the plates up to the centre of the Rayleigh cell, one can measure the mean temperature at only one or two different distances from the plate, and thus fix the best-fit coefficients in exponential approximation (4.10). In the case of the operating fluid water and for considered Ra, only two different measurements are required to represent the temperature distributions within the TBLs and in the whole cell with an error less than 0.5 % and 3.4 %, respectively.

To check the quality of the derived universal exponential approximation (4.11) of the mean temperature profiles for other fluids and geometries of the Rayleigh cell in the Boussinesq case, and to approximate the profiles for different fluids and Ra in non-Boussinesq case, further highly accurate measurements and DNS are required.

The authors are very grateful to Guenter Ahlers, Detlef Lohse, Ronald du Puits, Christian Resagk, Jörg Schumacher and Claus Wagner for useful comments. André Thess is grateful to the Deutsche Forschungsgemeinschaft for partial support of this work under grant Th 497/22-1.

REFERENCES

Ahlers, G. 2000 Effect of sidewall conductance on heat-transport measurements for turbulent Rayleigh–Bénard convection. *Phys. Rev.* E **63**, 015303.

Ahlers, G., Grossmann, S. & Lohse, D. 2009 Heat transfer and large-scale dynamics in turbulent Rayleigh–Bénard convection. *Rev. Mod. Phys.* **81**, 503–537.

Amati, G., Koal, K., Massaioli, F., Sreenivasan, K. R. & Verzicco, R. 2005 Turbulent thermal convection at high Rayleigh numbers for a Boussinesq fluid of constant Prandtl number. *Phys. Fluids* **17**, 121701.

Bodenschatz, E., Pesch, W. & Ahlers, G. 2000 Recent developments in Rayleigh–Bénard convection. *Annu. Rev. Fluid Mech.* **32**, 709–778.

Buschmann, M. & Gad-el-Hak, M. 2003 Debate concerning the mean-velocity profile of a turbulent boundary layer. *AIAA J.* **41**, 565–572.

Calzavarini, E., Lohse, D., Toschi, F. & Tripiccione, R. 2005 Rayleigh and Prandtl number scaling in the bulk of Rayleigh–Bénard turbulence. *Phys. Fluids* **17**, 055107.

Castaing, B., Gunaratne, G., Heslot, F., Kadanoff, L., Libchaber, A., Thomae, S., Wu, X. Z., Zaleski, S. & Zanetti, G. 1989 Scaling of hard thermal turbulence in Rayleigh–Bénard convection. *J. Fluid Mech.* **204**, 1–30.

Chilla, F., Ciliberto, S., Innocenti, C. & Pampaloni, E. 1993 Boundary layer and scaling properties in turbulent thermal convection. *Nuovo Cimento* **15**, 1229–1249.

Emran, M. S. & Schumacher, J. 2008 Fine-scale statistics of temperature and its derivatives in convective turbulence. *J. Fluid Mech.* **611**, 13–34.

Funfschilling, D., Brown, E., Nikolaenko, A. & Ahlers, G. 2005 Heat transport by turbulent Rayleigh–Bénard convection in cylindrical samples with aspect ratio one and larger. *J. Fluid Mech.* **536**, 145–154.

Grötzbach, G. 1983 Spatial resolution requirements for direct numerical simulation of Rayleigh–Bénard convection. *J. Comput. Phys.* **49**, 241–264.

Grossmann, S. & Lohse, D. 2000 Scaling in thermal convection: a unifying theory. *J. Fluid Mech.* **407**, 27–56.

Hartlep, T., Tilgner, A. & Busse, F. H. 2005 Transition to turbulent convection in a fluid layer heated from below at moderate aspect ratio. *J. Fluid Mech.* **544**, 309–322.

Hölling, M. & Herwig, H. 2006 Asymptotic analysis of heat transfer in turbulent Rayleigh–Bénard convection. *Intl J. Heat Mass Transfer* **49**, 1129–1136.

Kaczorowski, M. & Wagner, C. 2009 Analysis of the thermal plumes in turbulent Rayleigh–Bénard convection based on well-resolved numerical simulations. *J. Fluid Mech.* **618**, 89–112.

Kadanoff, L. P. 2001 Turbulent heat flow: structures and scaling. *Phys. Today* **54**, 34–39.

Kenjereš, S. & Hanjalić, K. 2006 LES, T-RANS and hybrid simulations of thermal convection at high Ra numbers. *Intl J. Heat Fluid Flow* **27**, 800–810.

Kerr, R. M. 1996 Rayleigh number scaling in numerical convection. *J. Fluid Mech.* **310**, 139–179.

Landau, L. D. & Lifshitz, E. M. 1959 *Fluid Mechanics.* Pergamon.

Lui, S.-L. & Xia, K.-Q. 1998 Spatial structure of the thermal boundary layer in turbulent convection. *Phys. Rev.* E **57**, 5494–5503.

Niemela, J. J. & Sreenivasan, K. R. 2003 Confined turbulent convection. *J. Fluid Mech.* **481**, 355–384.

du Puits, R., Resagk, C., Tilgner, A., Busse, F. H. & Thess, A. 2007 Structure of thermal boundary layers in turbulent Rayleigh–Bénard convection. *J. Fluid Mech.* **572**, 231–254.

van Reeuwijk, M., Jonker, H. J. J. & Hanjalić, K. 2008*a* Wind and boundary layers in Rayleigh–Bénard convection. I. Analysis and modeling. *Phys. Rev.* E **77**, 036311.

van Reeuwijk, M., Jonker, H. J. J. & Hanjalić, K. 2008*b* Wind and boundary layers in Rayleigh–Bénard convection. II. Boundary layer character and scaling. *Phys. Rev.* E **77**, 036312.

Schlichting, H., & Gersten, K. 2000 *Boundary Layer Theory*, 8th edn. Springer Verlag.

Sergent, A., Joubert, P. & Le Quéré, P. 2006 Large Eddy Simulation of turbulent thermal convection using a mixed scale diffusivity model. *Prog. Comp. Fluid Dyn.* **6**, 40–49.

Shishkina, O., Shishkin, A. & Wagner, C. 2009 Simulation of turbulent thermal convection in complicated domains. *J. Comput. Appl. Math.* **226**, 336–344.

Shishkina, O. & Wagner, C. 2007 Local heat fluxes in turbulent Rayleigh–Bénard convection. *Phys. Fluids* **19**, 085107.

Shishkina, O. & Wagner, C. 2008 Analysis of sheet-like thermal plumes in turbulent Rayleigh–Bénard convection. *J. Fluid Mech.* **599**, 383–404.

Shraiman, B. I. & Siggia, E. D. 1990 Heat transport in high-Rayleigh-number convection. *Phys. Rev.* A **42**, 3650–3653.

Siggia, E. D. 1994 High Rayleigh number convection. *Annu. Rev. Fluid Mech.* **26**, 137–168.

Tilgner, A., Belmonte, A. & Libchaber, A. 1993 Temperature and velocity profiles of turbulence convection in water. *Phys. Rev.* E **47** R2253–R2256.

Verzicco, R. & Camussi, R. 2003 Numerical experiments on strongly turbulent thermal convection in a slender cylindrical cell. *J. Fluid Mech.* **477**, 19–49.

Zanoun, E. S., Durst, F. & Nagib, H. 2003 Evaluating the law of the wall in two-dimensional fully developed turbulent channel flows. *Phys. Fluids* **15**, 3081–3089.

Zhou, Q., Sun, C. & Xia, K.-Q. 2007 Morphological evolution of thermal plumes in turbulent Rayleigh–Bénard convection. *Phys. Rev. Lett.* **98**, 074501.